Search for $Z' \to \mu^+\mu^-$ in the $L_\mu - L_\tau$ gauge-symmetric model at Belle

T. Czank,[38] I. Jaegle,[10,85] A. Ishikawa,[19,15] I. Adachi,[19,15] K. Adamczyk,[63] H. Aihara,[88] D. M. Asner,[3] T. Aushev,[21] R. Ayad,[82] V. Babu,[8] S. Bahinipati,[25] P. Behera,[28] J. Bennett,[53] F. Bernlochner,[2] M. Bessner,[18] V. Bhardwaj,[24] B. Bhuyan,[26] T. Bilka,[5] J. Biswal,[36] A. Bobrov,[4,67] G. Bonvicini,[93] A. Bozek,[63] M. Bračko,[50] T. E. Browder,[18] M. Campajola,[33,58] L. Cao,[2] D. Červenkov,[5] M.-C. Chang,[11] A. Chen,[60] B. G. Cheon,[17] K. Chilikin,[45] H. E. Cho,[17] K. Cho,[40] Y. Choi,[80] S. Choudhury,[27] D. Cinabro,[93] S. Das,[49] N. Dash,[28] G. De Nardo,[33,58] R. Dhamija,[27] F. Di Capua,[33,58] Z. Doležal,[5] T. V. Dong,[12] S. Eidelman,[4,67,45] T. Ferber,[8] D. Ferlewicz,[52] B. G. Fulsom,[69] R. Garg,[70] V. Gaur,[92] A. Garmash,[4,67] A. Giri,[27] P. Goldenzweig,[37] B. Golob,[46,36] O. Grzymkowska,[63] Y. Guan,[7] K. Gudkova,[4,67] C. Hadjivasiliou,[69] O. Hartbrich,[18] K. Hayasaka,[65] H. Hayashii,[59] M. T. Hedges,[18] M. Hernandez Villanueva,[53] T. Higuchi,[38] W.-S. Hou,[62] C.-L. Hsu,[81] T. Iijima,[57,56] K. Inami,[56] G. Inguglia,[31] R. Itoh,[19,15] M. Iwasaki,[68] Y. Iwasaki,[19] W. W. Jacobs,[29] E.-J. Jang,[16] S. Jia,[12] Y. Jin,[88] C. W. Joo,[38] K. K. Joo,[6] K. H. Kang,[43] G. Karyan,[8] T. Kawasaki,[39] H. Kichimi,[19] C. Kiesling,[51] B. H. Kim,[76] C. H. Kim,[17] D. Y. Kim,[79] K.-H. Kim,[95] S. H. Kim,[76] Y.-K. Kim,[95] P. Kodyš,[5] I. Komarov,[8] T. Konno,[39] A. Korobov,[4,67] S. Korpar,[50] E. Kovalenko,[4,67] P. Križan,[46,36] R. Kroeger,[53] P. Krokovny,[4,67] T. Kuhr,[47] M. Kumar,[49] K. Kumara,[93] Y.-J. Kwon,[95] Y.-T. Lai,[38] J. S. Lange,[13] I. S. Lee,[17] S. C. Lee,[43] Y. B. Li,[71] L. Li Gioi,[51] J. Libby,[28] K. Lieret,[47] D. Liventsev,[93,19] T. Luo,[12] C. MacQueen,[52] M. Masuda,[87,73] T. Matsuda,[54] D. Matvienko,[4,67,45] M. Merola,[33,58] F. Metzner,[37] K. Miyabayashi,[59] R. Mizuk,[45,21] G. B. Mohanty,[83] S. Mohanty,[83,91] T. Mori,[56] M. Mrvar,[31] R. Mussa,[34] M. Nakao,[19,15] Z. Natkaniec,[63] A. Natochii,[18] L. Nayak,[27] M. Niiyama,[42] N. K. Nisar,[3] S. Nishida,[19,15] H. Ono,[64,65] Y. Onuki,[88] P. Pakhlov,[45,55] G. Pakhlova,[21,45] T. Pang,[72] S. Pardi,[33] H. Park,[43] S.-H. Park,[19] S. Patra,[24] S. Paul,[84,51] T. K. Pedlar,[48] R. Pestotnik,[36] L. E. Piilonen,[92] T. Podobnik,[46,36] V. Popov,[21] E. Prencipe,[22] M. T. Prim,[2] M. Röhrken,[8] A. Rostomyan,[8] N. Rout,[28] G. Russo,[58] D. Sahoo,[83] S. Sandilya,[27] A. Sangal,[7] L. Santelj,[46,36] T. Sanuki,[86] V. Savinov,[72] G. Schnell,[1,23] J. Schueler,[18] C. Schwanda,[31] Y. Seino,[65] K. Senyo,[94] M. E. Sevior,[52] M. Shapkin,[32] C. Sharma,[49] V. Shebalin,[18] C. P. Shen,[12] J.-G. Shiu,[62] B. Shwartz,[4,67] A. Sokolov,[32] E. Solovieva,[45] S. Stanič,[66] M. Starič,[36] Z. S. Stottler,[92] M. Sumihama,[14] T. Sumiyoshi,[90] W. Sutcliffe,[2] M. Takizawa,[77,20,74] K. Tanida,[35] Y. Tao,[10] F. Tenchini,[8] K. Trabelsi,[44] M. Uchida,[89] S. Uehara,[19,15] T. Uglov,[45,21] K. Uno,[65] S. Uno,[19,15] P. Urquijo,[52] R. Van Tonder,[2] G. Varner,[18] A. Vossen,[9] C. H. Wang,[61] E. Wang,[72] M.-Z. Wang,[62] P. Wang,[30] S. Watanuki,[44] E. Won,[41] X. Xu,[78] B. D. Yabsley,[81] H. Yamamoto,[86] W. Yan,[75] S. B. Yang,[41] H. Ye,[8] J. Yelton,[10] J. H. Yin,[41] Y. Yusa,[65] Z. P. Zhang,[75] V. Zhilich,[4,67] V. Zhukova,[45] and V. Zhulanov[4,67]

(Belle Collaboration)

[1]*Department of Physics, University of the Basque Country UPV/EHU, 48080 Bilbao*
[2]*University of Bonn, 53115 Bonn*
[3]*Brookhaven National Laboratory, Upton, New York 11973*
[4]*Budker Institute of Nuclear Physics SB RAS, Novosibirsk 630090*
[5]*Faculty of Mathematics and Physics, Charles University, 121 16 Prague*
[6]*Chonnam National University, Gwangju 61186*
[7]*University of Cincinnati, Cincinnati, Ohio 45221*
[8]*Deutsches Elektronen–Synchrotron, 22607 Hamburg*
[9]*Duke University, Durham, North Carolina 27708*
[10]*University of Florida, Gainesville, Florida 32611*
[11]*Department of Physics, Fu Jen Catholic University, Taipei 24205*
[12]*Key Laboratory of Nuclear Physics and Ion-beam Application (MOE) and Institute of Modern Physics, Fudan University, Shanghai 200443*
[13]*Justus-Liebig-Universität Gießen, 35392 Gießen*
[14]*Gifu University, Gifu 501-1193*
[15]*SOKENDAI (The Graduate University for Advanced Studies), Hayama 240-0193*
[16]*Gyeongsang National University, Jinju 52828*
[17]*Department of Physics and Institute of Natural Sciences, Hanyang University, Seoul 04763*
[18]*University of Hawaii, Honolulu, Hawaii 96822*
[19]*High Energy Accelerator Research Organization (KEK), Tsukuba 305-0801*
[20]*J-PARC Branch, KEK Theory Center, High Energy Accelerator Research Organization (KEK), Tsukuba 305-0801*
[21]*Higher School of Economics (HSE), Moscow 101000*
[22]*Forschungszentrum Jülich, 52425 Jülich*

[23]*IKERBASQUE, Basque Foundation for Science, 48013 Bilbao*
[24]*Indian Institute of Science Education and Research Mohali, SAS Nagar 140306*
[25]*Indian Institute of Technology Bhubaneswar, Satya Nagar 751007*
[26]*Indian Institute of Technology Guwahati, Assam 781039*
[27]*Indian Institute of Technology Hyderabad, Telangana 502285*
[28]*Indian Institute of Technology Madras, Chennai 600036*
[29]*Indiana University, Bloomington, Indiana 47408*
[30]*Institute of High Energy Physics, Chinese Academy of Sciences, Beijing 100049*
[31]*Institute of High Energy Physics, Vienna 1050*
[32]*Institute for High Energy Physics, Protvino 142281*
[33]*INFN—Sezione di Napoli, 80126 Napoli*
[34]*INFN—Sezione di Torino, 10125 Torino*
[35]*Advanced Science Research Center, Japan Atomic Energy Agency, Naka 319-1195*
[36]*J. Stefan Institute, 1000 Ljubljana*
[37]*Institut für Experimentelle Teilchenphysik, Karlsruher Institut für Technologie, 76131 Karlsruhe*
[38]*Kavli Institute for the Physics and Mathematics of the Universe (WPI), University of Tokyo, Kashiwa 277-8583*
[39]*Kitasato University, Sagamihara 252-0373*
[40]*Korea Institute of Science and Technology Information, Daejeon 34141*
[41]*Korea University, Seoul 02841*
[42]*Kyoto Sangyo University, Kyoto 603-8555*
[43]*Kyungpook National University, Daegu 41566*
[44]*Université Paris-Saclay, CNRS/IN2P3, IJCLab, 91405 Orsay*
[45]*P.N. Lebedev Physical Institute of the Russian Academy of Sciences, Moscow 119991*
[46]*Faculty of Mathematics and Physics, University of Ljubljana, 1000 Ljubljana*
[47]*Ludwig Maximilians University, 80539 Munich*
[48]*Luther College, Decorah, Iowa 52101*
[49]*Malaviya National Institute of Technology Jaipur, Jaipur 302017*
[50]*Faculty of Chemistry and Chemical Engineering, University of Maribor, 2000 Maribor, Slovenia*
[51]*Max-Planck-Institut für Physik, 80805 München*
[52]*School of Physics, University of Melbourne, Victoria 3010*
[53]*University of Mississippi, University, Mississippi 38677*
[54]*University of Miyazaki, Miyazaki 889-2192*
[55]*Moscow Physical Engineering Institute, Moscow 115409*
[56]*Graduate School of Science, Nagoya University, Nagoya 464-8602*
[57]*Kobayashi-Maskawa Institute, Nagoya University, Nagoya 464-8602*
[58]*Università di Napoli Federico II, 80126 Napoli*
[59]*Nara Women's University, Nara 630-8506*
[60]*National Central University, Chung-li 32054*
[61]*National United University, Miao Li 36003*
[62]*Department of Physics, National Taiwan University, Taipei 10617*
[63]*H. Niewodniczanski Institute of Nuclear Physics, Krakow 31-342*
[64]*Nippon Dental University, Niigata 951-8580*
[65]*Niigata University, Niigata 950-2181*
[66]*University of Nova Gorica, 5000 Nova Gorica*
[67]*Novosibirsk State University, Novosibirsk 630090*
[68]*Osaka City University, Osaka 558-8585*
[69]*Pacific Northwest National Laboratory, Richland, Washington 99352*
[70]*Panjab University, Chandigarh 160014*
[71]*Peking University, Beijing 100871*
[72]*University of Pittsburgh, Pittsburgh, Pennsylvania 15260*
[73]*Research Center for Nuclear Physics, Osaka University, Osaka 567-0047*
[74]*Meson Science Laboratory, Cluster for Pioneering Research, RIKEN, Saitama 351-0198*
[75]*Department of Modern Physics and State Key Laboratory of Particle Detection and Electronics, University of Science and Technology of China, Hefei 230026*
[76]*Seoul National University, Seoul 08826*
[77]*Showa Pharmaceutical University, Tokyo 194-8543*
[78]*Soochow University, Suzhou 215006*
[79]*Soongsil University, Seoul 06978*
[80]*Sungkyunkwan University, Suwon 16419*

[81]School of Physics, University of Sydney, New South Wales 2006
[82]Department of Physics, Faculty of Science, University of Tabuk, Tabuk 71451
[83]Tata Institute of Fundamental Research, Mumbai 400005
[84]Department of Physics, Technische Universität München, 85748 Garching
[85]Thomas Jefferson National Accelerator Facility, Newport News Virginia 23606
[86]Department of Physics, Tohoku University, Sendai 980-8578
[87]Earthquake Research Institute, University of Tokyo, Tokyo 113-0032
[88]Department of Physics, University of Tokyo, Tokyo 113-0033
[89]Tokyo Institute of Technology, Tokyo 152-8550
[90]Tokyo Metropolitan University, Tokyo 192-0397
[91]Utkal University, Bhubaneswar 751004
[92]Virginia Polytechnic Institute and State University, Blacksburg, Virginia 24061
[93]Wayne State University, Detroit, Michigan 48202
[94]Yamagata University, Yamagata 990-8560
[95]Yonsei University, Seoul 03722

(Received 20 September 2021; accepted 28 June 2022; published 8 July 2022)

We search for a new gauge boson Z' that couples only to heavy leptons and their corresponding neutrinos in the process $e^+e^- \to Z'(\to \mu^+\mu^-)\mu^+\mu^-$, using a 643 fb^{-1} data sample collected by the Belle experiment at or near the $\Upsilon(1S, 2S, 3S, 4S, 5S)$ resonances at the KEKB collider. While previous searches for Z' performed a data-based estimation of the initial state radiation effect, our search for the Z' is the first to include effects due to initial state radiation in the signal simulated samples that were used in estimating the detection efficiency. No signal is observed in the Z' mass range of 0.212–10 GeV/c^2, and we set an upper limit on the coupling strength, g', constraining the possible Z' contribution to the anomalous magnetic dipole moment of the muon.

DOI: 10.1103/PhysRevD.106.012003

I. INTRODUCTION

The lack of evidence for a weakly interacting massive particle by underground experiments [1,2] and the absence of supersymmetric particle signals at the LHC [3–5] suggest that dark matter might be composite and/or light. This gives rise to dark sector models [6–16] that introduce a zoology of dark particles which do not interact directly via Standard Model (SM) forces but can interact by dark sector forces via new mediators. Therefore, they interact only indirectly with SM particles and could have masses between 1 MeV/c^2 and 10 GeV/c^2.

Discrepancies observed at low-energy measurements [17,18] have fueled new precision studies. Within this context, the anomalous magnetic moment of the muon, $(g-2)_\mu$, is one of the most precisely measured quantities in particle physics, where the difference between the experimental value and the SM prediction [19] is about 4.2σ [20]. This discrepancy might be a sign of new physics and has led to a variety of attempts to create physics models involving the leptonic sector of the SM [21–24].

These attempts include the set of SM extensions that add a new $U(1)$ gauge boson (Z') coupled to the difference between lepton family numbers, L_i where $i = e$, μ, and τ [22]. The electron number differences have been well constrained by measurements performed at e^+e^- colliders [25,26] and will not be discussed here. In this study, we present a search for the gauge boson coupled to the $L_\mu - L_\tau$ difference.

The partial widths for the Z' decay to leptons [27,28] are given by

$$\Gamma(Z' \to \ell^+\ell^-) = \frac{(g')^2 M_{Z'}}{12\pi}\left(1+\frac{2M_\ell^2}{M_{Z'}^2}\right) \times \sqrt{1-\frac{4M_\ell^2}{M_{Z'}^2}}\theta(M_{Z'}-2M_\ell), \quad (1)$$

where g' is the $L_\mu - L_\tau$ coupling strength, and $\theta(M_{Z'}-2M_\ell)$ is a step function, and

$$\Gamma(Z' \to \nu_\ell \bar{\nu}_\ell) = \frac{(g')^2 M_{Z'}}{24\pi}. \quad (2)$$

For $M_{Z'} \gg M_\ell$, the branching fraction to one neutrino flavor is half of that to a charged lepton. This is due to the fact that the Z' boson only couples to left-handed neutrinos, but couples to both left- and right-handed charged leptons.

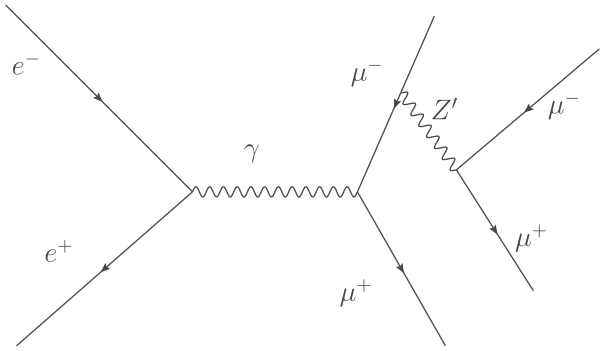

FIG. 1. Feynman diagram for the main production channel of the Z' in e^+e^- colliders.

The visible branching fraction to muons is

$$\mathcal{B}(Z' \to \mu^+\mu^-) = \frac{\Gamma(Z' \to \mu^+\mu^-)}{\sum_{\ell}^{\mu,\tau}(\Gamma(Z' \to \nu_\ell \bar{\nu}_\ell) + \Gamma(Z' \to \ell^+\ell^-))}, \tag{3}$$

which is identical to $\mathcal{B}(Z' \to \tau\tau)$ except for the replacement of the decay width with the appropriate decay channel.

We search for the Z' of an $L_\mu - L_\tau$ model via the decay $Z' \to \mu^+\mu^-$. In this model, the Z' only couples to the second and third generation of leptons (μ, τ) and their neutrinos. We search for four-muon events in the reaction depicted in Fig. 1, in which the $e^+e^- \to \mu^+\mu^-$ process is followed by Z' radiation from a muon, and then, the Z' decays to $\mu^+\mu^-$.

In addition to its possible contribution to the $(g-2)_\mu$ anomaly, the effects of a Z' have been searched for in other scenarios. It could be a source of an increase in the neutrino trident production, $\nu_\mu N \to N\nu_\mu\mu^+\mu^-$ [23]. No increase has been observed, and a limit was set for the Z' parameter space. It could also work as an indirect channel to sterile neutrino dark matter [24] and could provide predictions for the neutrino mass-mixing matrix [29–31].

Recently, the Belle II Collaboration published the search result with $Z' \to \nu\nu$ decay using a 276 pb^{-1} luminosity data [32]. No Z' signature was found so an upper limit of the parameter space of this decay mode was set. Previously, *BABAR* searched for the Z' with $e^+e^- \to Z'(\to \mu^+\mu^-)\mu^+\mu^-$ using a 514 fb^{-1} luminosity data, and since no Z' signature was found, the most stringent upper limits as a function of Z' mass [33] were set. In this paper, we present a search for the same Z' model in the full available Belle data sample.

II. EXPERIMENTAL SETUP

The search for $e^+e^- \to \mu^+\mu^- Z'(\to \mu^+\mu^-)$ is performed using the following luminosities: 33 fb^{-1} taken at the $\Upsilon(1S)$ and $\Upsilon(2S)$ resonances, 2 fb^{-1} at the $\Upsilon(3S)$ resonance, 484 fb^{-1} at the $\Upsilon(4S)$ resonance, 93 fb^{-1} at the $\Upsilon(5S)$ resonance, and 67 fb^{-1} taken 60 MeV below the $\Upsilon(4S)$ resonance, totaling 679 fb^{-1} collected by the Belle detector [34,35] at the KEKB collider [36,37]. A 36 fb^{-1} subset of the $\Upsilon(4S)$ sample, the validation sample, is used to verify the selection criteria and then discarded from the analysis.

The Belle detector surrounds the interaction point of KEKB. It is a large-solid-angle magnetic spectrometer consisting of a silicon vertex detector, a 50-layer central drift chamber (CDC), an array of aerogel threshold Cherenkov counters, a barrellike arrangement of time-of-flight scintillation counters, and an electromagnetic calorimeter (ECL) comprised of CsI(TI) crystals located inside a superconducting solenoid coil that provides a 1.5 T magnetic field. An iron flux return located outside of the coil is instrumented with resistive plate chambers to detect K_L^0 mesons and identify muons (KLM). The signal events are guaranteed to pass the trigger with nearly full efficiency because the muonic Z' decay topology features more than three charged tracks. In addition, the large radius of the CDC (880 mm) [38] allows for an excellent mass resolution and muon detection efficiency in Belle.

III. SELECTION CRITERIA

The selection is optimized based on the validation sample as well as a Monte Carlo (MC) simulation done in two steps. First, signal events are generated for different Z' mass hypotheses using WHIZARD [39], which takes into account the initial state radiation (ISR) as well as the final state radiation (FSR) at the $\Upsilon(4S)$ center-of-mass energy. WHIZARD also has an option to generate events without radiative corrections. Then, the detector response to these events is simulated using GEANT3 [40]. There were 54 mass hypotheses generated for each of the Z' MC samples from $m_{Z'} = 212$ MeV/c^2 to $m_{Z'} = 1.015$ GeV/c^2 in 100 MeV/c^2 steps and subsequently, in 200 MeV/c^2 steps up to $m_{Z'} = 10.00$ GeV/c^2. The change in the steps is due to the behavior of the detection efficiency observed in the analysis.

The irreducible background, $e^+e^- \to \mu^+\mu^-\mu^+\mu^-$ is studied with an MC sample corresponding to a luminosity of 336 fb^{-1} generated with `Diag36` [41] at $\Upsilon(4S)$ center-of-mass energy; `Diag36` generates events without ISR corrections (non-ISR). There is no event generator available for the QED 4-lepton final state with radiative correction. In addition, other leptonic and hadronic background sources, such as $e^+e^- \to e^+e^-e^+e^-$ and $e^+e^- \to \pi^+\pi^- J/\psi(\to \mu^+\mu^-)$ were studied through MC samples, and found to give negligible or no contributions after the application of the selection criteria.

We select events with two pairs of oppositely charged tracks in the final state. To ensure these tracks originate from the interaction point, their transverse and longitudinal impact parameters must be less than 0.2 and 1.5 cm, respectively. At least two tracks are required to have a

muon likelihood ratio, $\frac{\mathcal{L}_\mu}{\mathcal{L}_\mu+\mathcal{L}_K+\mathcal{L}_\pi}$, greater than 0.1. The value of $\mathcal{L}_\mu$ depends on the difference between the expected and actual muon penetration of the track in the KLM, and the distance between its KLM hits and the extrapolation of the track from the CDC. The efficiency for a track to be identified as a muon is about 95% for momenta between 1 to 3 GeV/c and a slightly lower momenta below 1 GeV/c. In addition, a hadron veto is applied. The muon candidate must not have a likelihood ratio corresponding to a pion, kaon, or a proton. This is implemented by comparing the likelihood ratio of two particles (proton and kaon, kaon and pion, and proton and pion) as $P(i|j) = \frac{\mathcal{L}_i}{\mathcal{L}_i+\mathcal{L}_j}$, where $\mathcal{L}_i$ is the likelihood product from three detectors (ACC, TOF, and CDC). A pion is defined as $P(K|\pi) < 0.4$ and $P(p|\pi) < 0.4$. A kaon is defined as $P(p|K) < 0.4$ and $P(K|i) > 0.6$. A proton is defined as $P(p|K) > 0.6$ and $P(p|\pi) > 0.6$.

To suppress the background due to neutral particles, the sum of ECL clusters unrelated to any charged tracks with an energy greater than 30 MeV is required to be less than 200 MeV. Additionally, the visible energy, $E_{\rm vis}$, calculated from the four muons must be consistent with the center-of-mass energy, $E_{\rm CMS}$, so that $|E_{\rm CMS} - E_{\rm vis}| < 500$ MeV.

A kinematic fit based on the least square method for the final state is carried out under the constraint that the four-momentum of the final state be compatible with the initial e^+e^- system. The chi-squared is minimized by Lagrange multipliers; they issue a set of nonlinear equations that are solved using the multidimensional Newton-Raphson method. As a result, the reconstructed Z' mass resolution is improved.

As there are four possible combinations of oppositely charged muons in the final state, all four possible combinations correspond to four Z' candidates counted per event. To improve the sensitivity in the low Z' mass region, we introduce a reduced mass, defined as $m_R = \sqrt{m^2_{\mu^+\mu^-} - 4m^2_{\mu,\rm PDG}}$, where $m_{\mu\mu}$ is the invariant masses of Z' candidate and $m^2_{\mu,\rm PDG}$ is the muon nominal mass [42]. The m_R distribution is smoother than the invariant mass distribution around the Z' mass close to the dimuon threshold.

The Z' reduced mass distributions for data and MC are compared in Fig. 2. Although the normalization of the data is almost 70% of the background level, it is fit to a constant probability density function (pdf) as shown in Fig. 2 (bottom). This difference arises due to the ISR effect, which is not simulated in the background MC sample.

We veto the reduced mass distribution around the J/ψ mass, $3.05 < m_R < 3.13$ GeV/c^2, as its muonic decay can mimic a signal. This was not necessary around the $\psi(2S)$ mass since the $\psi(2S)$ decay into muons is negligible compared to the main background.

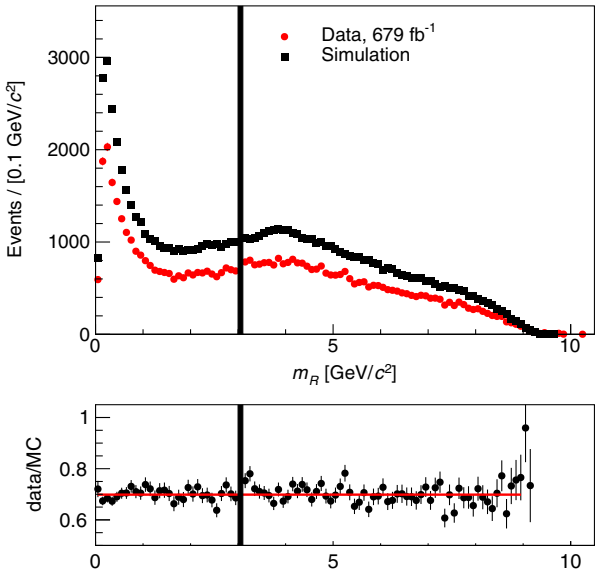

FIG. 2. Top: Reduced mass, m_R, distributions. Red points represent the data after all selection criteria are applied. Black squares represent the non-ISR MC expectation for the $e^+e^- \to \mu^+\mu^-\mu^+\mu^-$ (Diag36) [41] scaled to the data luminosity. Bottom: The ratio between data and the non-ISR $e^+e^- \to \mu^+\mu^-\mu^+\mu^-$ MC expectation. The red line represents a fit of a first order polynomial where its constant term is 0.700 ± 0.003 and the slope term is negligible. Both: Black shaded region at 3.1 GeV/c^2 represents the J/ψ region which is not used in this analysis.

IV. RESULTS

We perform a binned maximum-likelihood fit to the reduced mass distribution with the range of $m_{Z'} \pm 25\sigma_{Z'}$. The fit is repeated 9788 times with a different Z' mass hypotheses in steps of 1 MeV/c^2 from 0 to 9787 MeV/c^2. The Z' resolution starts from less than 1 MeV/c^2 at the dimuon mass threshold increasing until 5.5 GeV/c^2, where it is valued at 6 MeV/c^2. Then it starts decreasing until 9.5 GeV/c^2 where it is valued at ~3 MeV/c^2. The step is set around half of the width of the reduced mass distribution for MC generated signal.

The signal m_R distribution is modeled as a sum of two Crystal Ball [43] functions with a common mean. The shape parameters as a function of the m_R are determined with signal MC samples while the normalization is floated in the fit. The width is calibrated using $J/\psi \to \mu^+\mu^-$ events in the veto region. The background is modeled with a third-order polynomial, which is the lowest order function that can fit the $e^+e^- \to \mu^+\mu^-\mu^+\mu^-$ background well. Background normalization and shape parameters are floated in the fit.

The efficiency is determined using a fit to the MC signal samples with different mass hypotheses. It is the result of the integration of the fit function over $m_{Z'} \pm 3\sigma_{Z'}$, where $\sigma_{Z'}$ is the Z' mass resolution. This efficiency is interpolated between the different discrete mass hypotheses.

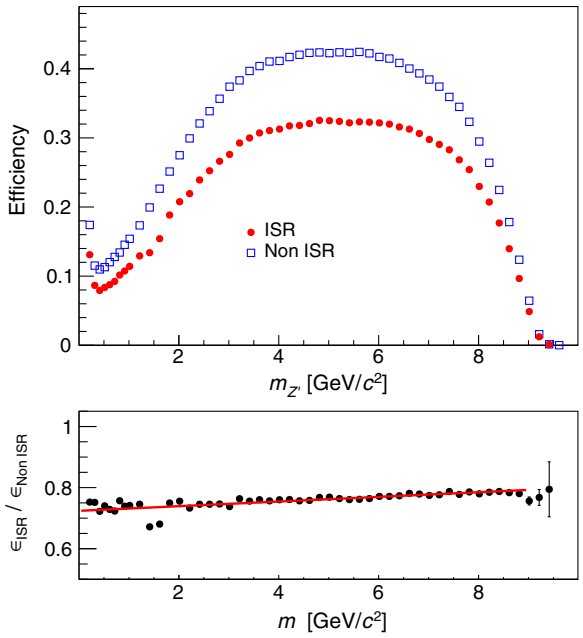

FIG. 3. Top: Detection efficiency as a function of the reduced mass. Red points represent values with ISR correction. Open blue squares represent values without it. Bottom: Ratio between ISR and non-ISR detection efficiencies linearly fit. The average constant value from a linear and constant fit is 0.741 ± 0.001.

This procedure is done identically for non-ISR MC samples where the m_R distribution is also modeled as a sum of two Crystal Ball functions with a common mean; however, for the non-ISR MC samples, the parametrization of the pdf is different than for the ISR case. Comparing ISR and non-ISR detection efficiencies is key to understand the gap between data and MC background on Fig. 2.

Figure 3 shows efficiencies as a function of reduced mass.

It is clear that the detection efficiency increases with increasing Z' mass up to 6 GeV/c^2, and then it decreases. This behavior is due to the muon detection efficiency in the KLM, which has a threshold momentum of 600 MeV/c reaching maximum at 1 GeV/c, then flattens for even higher values.

Systematic uncertainties arise from luminosity, track identification, muon identification, and fitting bias. The luminosity uncertainty is 1.4% and is measured using Bhabha and two-photon events. The track identification uncertainty is 0.35% per charged track, or 1.4% in this analysis, and is determined by comparing the track finding efficiency of partially and fully reconstructed $D^{*+} \to D^0(\to K^-\pi^+)\pi^+$ decays. A muon identification uncertainty of 1.15% is determined from the change in event yields while varying the muon likelihood ratio criterion from 0.1 to 0.2. With muon likelihood cuts, there is also a systematic error to be considered on the detection efficiency calculated through MC signal samples. This error is calculated comparing $\gamma\gamma \to \mu^+\mu^-$ data and MC samples. Due to the large number of these events, it is possible to map the dependency between momentum, muon likelihood ratio, and error rate. Comparing our MC signal calculated detection efficiency with and without this correction gives a 1% difference. Finally, a correction from the hadron veto is implemented on the MC samples. This correction factor is also 1%, and it is obtained by comparing MC samples with and without the hadron veto.

The effect of fitting bias is investigated using a bootstrap study to check whether allowing third-order polynomial components to float in the fit end up inducing a bias on the yield extracted. For each mass scan, this study is done by varying the data with a Poisson distribution, varying each individual bin of the histogram. This changed dataset is then injected with a signal of yield, corresponding to a Poisson distribution of the upper limit on the number of observed events and a distribution following its pdf. This reconstructed ensemble is then fitted in the same way as the data. The newly extracted yield, $\mathrm{N_{sig}}$, is then compared to the true number of events injected, $N_{\mathrm{sig}}^{\mathrm{true}}$, divided by the uncertainty in the newly yield extracted, $\sigma_{\mathrm{N_{sig}}}$, as $(\mathrm{N_{sig}^{true}} - \mathrm{N_{sig}})/\sigma_{\mathrm{N_{sig}}}$. This procedure is repeated 1000 times for each mass scan. We find that the extracted yield and its uncertainty are systematically overestimated by 3% and 4%, respectively. These biases are accordingly taken into account in the Z' scan and g' upper limit calculation by correcting the yield extracted and the error on the yield extracted. They correspond to $N_{\mathrm{sig}}^{\mathrm{cor}} = N_{\mathrm{sig}}(1+b)$ and $N_{\mathrm{sig}}^{\mathrm{errcor}} = N_{\mathrm{sig}}^{\mathrm{err}} \times b^{\mathrm{err}}$, where b stands for bias and the variables with a superscript err are related to the error on the yield.

The significance of each possible Z' candidate is evaluated as

$$\mathcal{S} = \mathrm{sign}(N_{\mathrm{obs}})\sqrt{2\log(\mathcal{L}_{\mathrm{S+B}}/\mathcal{L}_{\mathrm{B}})}, \tag{4}$$

where $\mathrm{sign}(N_{\mathrm{obs}})$ is the sign of the number of observed events and $\mathcal{L}_{\mathrm{S+B}}/\mathcal{L}_{\mathrm{B}}$ is the ratio between the maximum likelihoods of the fits with a signal plus background hypothesis $(\mathcal{L}_{\mathrm{S+B}})$ and background only hypothesis $(\mathcal{L}_{\mathrm{B}})$. The distribution of significances is shown Fig. 4.

The largest local significance observed in an excess (deficit) is 3.7σ (3.5σ) around $m_{Z'} = 3.3$ GeV/c^2 (3.1 GeV/c^2), in Fig. 5. After incorporating the look-elsewhere-effect, the global significance for the excess becomes 2.23σ.

Since no fit resulted in a global significance of at least 5σ, we set upper limits on the coupling strength g' as a function of $m_{Z'}$. A Bayesian method [44] is used to estimate the 90% credibility interval (C.I.) upper limit on the number of observed signal events, N_{obs}. A flat prior is assumed for the signal yield and two nuisance parameters are added, one for the signal yield and another for the background yield. These nuisance parameters are two Gaussian uncertainties

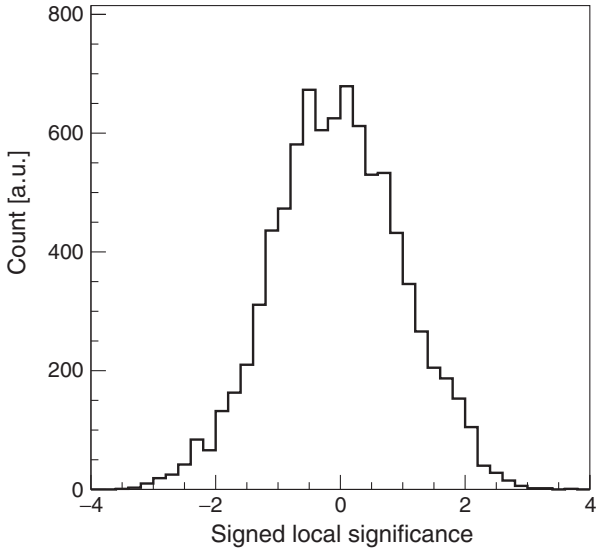

FIG. 4. Local signed significance values.

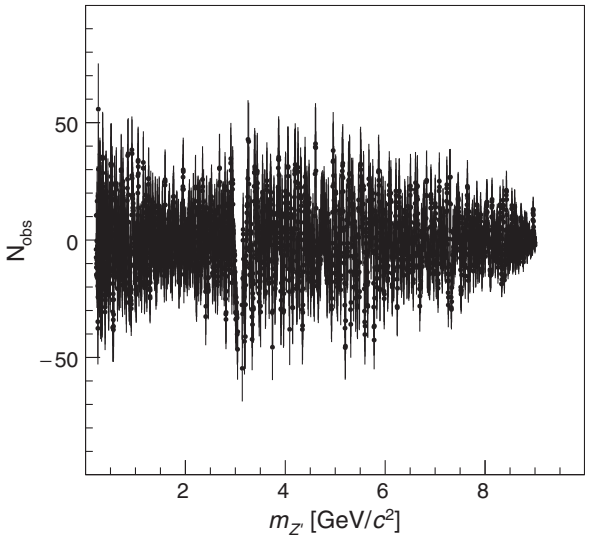

FIG. 6. Number of observed signal events (N_{obs}) from the fit for the different Z' mass hypotheses.

that correspond to the systematic errors. For the background nuisance parameter, the statistical errors are added in quadratic sum to the systematic errors [45].

The results are shown in Fig. 6. Using the calculated detection efficiency as shown in Fig. 3, the branching fraction from Eq. (3) and the Belle luminosity ($\mathcal{L}$) of 643 fb^{-1}, the 90% upper limit on the Born $e^+e^- \to Z'\mu^+\mu^-$ cross section is obtained using

$$\sigma_B = \frac{N_{obs}}{\mathcal{L}\mathcal{B}\epsilon_{ISR}(1+\delta)|1-\Pi|^2}, \tag{5}$$

where N_{obs}, ϵ_{ISR}, $\mathcal{B}$, $(1+\delta)$ and $|1-\Pi(s)|^2$ are the upper limit on the yield extracted from the data scan as shown in Fig. 6, the ISR signal MC sample based detection efficiency, the branching fraction from Eq. (3), the ISR correction factor, and the vacuum polarization factor, respectively.

In order to test the ISR and the vacuum polarization effects, we check the ratio between the number of observed signal N^S_{obs} and the number of simulated signal events N^S_{MC}. This can be written as

$$\frac{N^S_{obs}}{N^S_{MC}} = \frac{\sigma_V}{\sigma_B} \times \frac{\epsilon_{ISR}}{\epsilon_{non-ISR}}, \tag{6}$$

where $\epsilon_{ISR}(\epsilon_{non-ISR})$ is the detection efficiency obtained by the ISR (non-ISR) signal MC. Since the cross section with the ISR and vacuum polarization corrections (σ_V) is related to the Born cross section by $\sigma_V = (1+\delta)|1-\Pi|^2 \times \sigma_B$ [46] the ratio, Eq. (6), becomes

$$\frac{N^S_{obs}}{N^S_{MC}} = (1+\delta)|1-\Pi|^2 \times \frac{\epsilon_{ISR}}{\epsilon_{non-ISR}}. \tag{7}$$

As the ISR and vacuum polarization corrections are common for the signal and the $e^+e^- \to \mu^+\mu^-\mu^+\mu^-(4\mu)$ background process, one can expect that the ratio, Eq. (6), is the same for the signal and the 4μ background: $\frac{N^S_{obs}}{N^S_{MC}} = \frac{N^{4\mu}_{obs}}{N^{4\mu}_{MC}}$.

Checking the consistency of the efficiency and ISR correction factors can be carried out by the 4μ MC

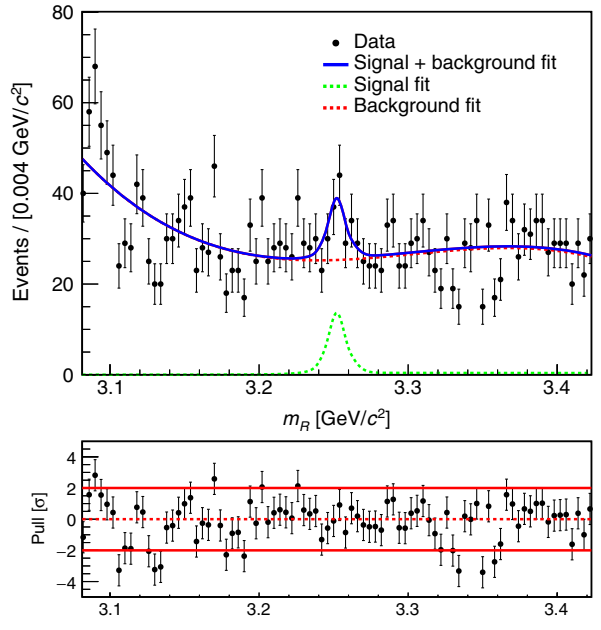

FIG. 5. The solid blue curve represents a fit to the data of a sum of two Crystal Ball functions added to a third-order polynomial. The dashed red and green curves represent the third-order polynomial and the sum of two Crystal Ball functions, respectively.

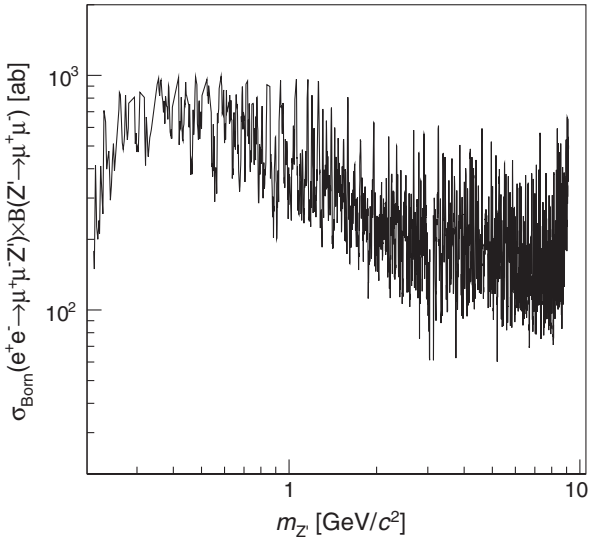

FIG. 7. 90% C.I. upper limit on the Born cross section for $e^+e^- \to \mu^+\mu^-(Z' \to \mu^+\mu^-)$ as a function of $m_{Z'}$.

background and data. From Fig. 2, we observe the ratio between data and the MC expectation for the 4μ process to be $\frac{N^S_{\rm obs.}}{N^{4\mu}_{\rm MC}} = 0.700$. This value is compatible with the product of the ratio of the detection efficiencies $(\frac{\epsilon_{\rm ISR}}{\epsilon_{\rm non-ISR}} = 0.741)$ and the ISR factor multiplied by the vacuum polarization $((1+\delta)(1-\Pi)^2 = 0.945)$.

The 90% C.I. upper limits on Born cross section as a function of $m_{Z'}$ are calculated and shown in Fig. 7.

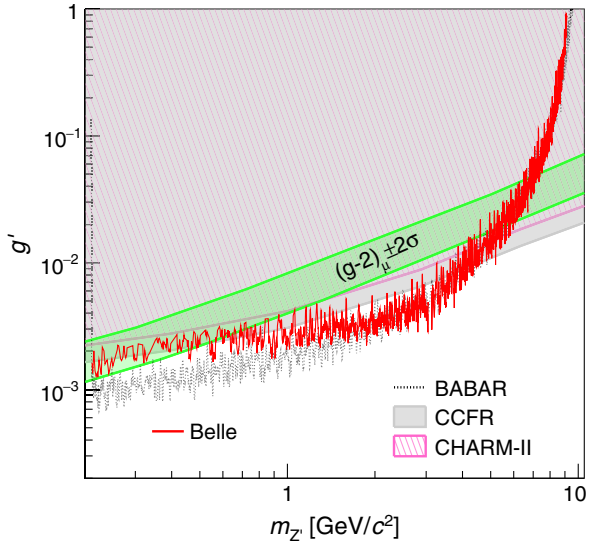

FIG. 8. 90% C.I. upper limit on g' as a function of $m_{Z'}$. The red solid is the Belle result. The black dotted line represents the *BABAR* results [33], the light gray shaded area is the result of CCFR, and the light purple hashed area is the result of CHARM-II over the Z' parameter space [23,48], and the green region indicates the values of the Z' coupling needed to explain $(g-2)_\mu$ suggested by the Muon $g-2$ Collaboration [17,20].

A. Limits on the coupling strength g'

With a Born theoretical cross section $\sigma_{\rm th}(\sqrt{s})$, for a given $m_{Z'}$, at $\sqrt{s}$ and the coupling g', the expected number of signal events for data samples used in this analysis is given as

$$N_{\rm exp} = g'^2 \varepsilon \mathcal{B}(\sigma^{\Upsilon(4S)}_{\rm th}(m_{Z'})\mathcal{L}^{\Upsilon(4S)} + \sigma^{\Upsilon(3S)}_{\rm th}\mathcal{L}^{\Upsilon(3S)} + \ldots). \quad (8)$$

With Eq. (8), the 90% C.I. upper limit on g' corresponding to $N_{\rm exp} = N_{\rm obs}$, is calculated and shown in Fig. 8. The result excludes most of the Z' parameter space that could be related to the updated $(g-2)_\mu$ region from the Muon $(g-2)$ experiment [17,20]. Also shown in Fig. 8 are comparisons with the CHARM-II experiment, the first measurement of the neutrino trident production [47], the reinterpretation of the Columbia-Chicago-Fermilab-Rochester (CCFR) results [23,48], and the first $Z' \to \mu^+\mu^-$ search done by *BABAR* [33].

V. CONCLUSION

In summary, we report a search for a new gauge boson Z' in the $L_\mu - L_\tau$ model with the on shell production of $e^+e^- \to Z'\mu^+\mu^-$, followed by $Z' \to \mu^+\mu^-$. This is the first search with the ISR effect directly included in the MC signal sample, since previous searches did a data-driven estimation of the ISR effect. Since no significant excess is observed, the upper limit on the coupling is set and the Z' parameter space constraint is improved.

This result specifically improves the previous g' upper limit between 2 and 8.4 GeV/c^2.

The Z' mass region lighter than the dimuon threshold, does not have any constraints, but in the future, Belle II will be able to perform a more stringent test for the region [49–51].

ACKNOWLEDGMENTS

We thank B. Shuve for providing the models for MadGraph5 and the branching fractions for Z'. Our gratitude goes to K. Mawatari for showing us the limitations of MadGraph5 when simulating ISR events and to J. Reuter for explaining how to use WHIZARD for generating ISR Z' events. We also thank T. Shimomura for the enlightening discussions about Z'. T. C. is supported by the Japan Society for the Promotion of Science (JSPS) Grant No. 20H05858 and A. I. is supported by Grants No. 16H02176 and No. 22H00144. We thank the KEKB group for the excellent operation of the accelerator; the KEK cryogenics group for the efficient operation of the solenoid; and the KEK computer group, and the Pacific Northwest National Laboratory (PNNL) Environmental Molecular Sciences Laboratory (EMSL) computing group for strong computing support; and the National Institute of Informatics, and Science Information

NETwork 5 (SINET5) for valuable network support. We acknowledge support from the Ministry of Education, Culture, Sports, Science, and Technology (MEXT) of Japan, the JSPS including Grant No. 20H05850, and the Tau-Lepton Physics Research Center of Nagoya University; the Australian Research Council including Grants No. DP180102629, No. DP170102389, No. DP170102204, No. DP150103061, No. FT130100303; Austrian Federal Ministry of Education, Science and Research (FWF) and FWF Austrian Science Fund No. P 31361-N36; the National Natural Science Foundation of China under Contracts No. 11435013, No. 11475187, No. 11521505, No. 11575017, No. 11675166, No. 11705209; Key Research Program of Frontier Sciences, Chinese Academy of Sciences (CAS), Grant No. QYZDJ-SSW-SLH011; the CAS Center for Excellence in Particle Physics (CCEPP); the Shanghai Pujiang Program under Grant No. 18PJ1401000; the Shanghai Science and Technology Committee (STCSM) under Grant No. 19ZR1403000; the Ministry of Education, Youth and Sports of the Czech Republic under Contract No. LTT17020; Horizon 2020 ERC Advanced Grant No. 884719 and ERC Starting Grant No. 947006 "InterLeptons" (European Union); the Carl Zeiss Foundation, the Deutsche Forschungsgemeinschaft, the Excellence Cluster Universe, and the VolkswagenStiftung; the Department of Atomic Energy (Project Identification No. RTI 4002) and the Department of Science and Technology of India; the Istituto Nazionale di Fisica Nucleare of Italy; National Research Foundation (NRF) of Korea Grants No. 2016R1D1A1B01010135, No. 2016R1D1A1B02012900, No. 2018R1A2B3003643, No. 2018R1A6A1A06024970, No. 2018R1D1A1B07047294, No. 2019K1A3A7A09033840, No. 2019R1I1A3A01058933; Radiation Science Research Institute, Foreign Large-size Research Facility Application Supporting project, the Global Science Experimental Data Hub Center of the Korea Institute of Science and Technology Information and KREONET/GLORIAD; the Polish Ministry of Science and Higher Education and the National Science Center; the Ministry of Science and Higher Education of the Russian Federation, Agreement No. 14.W03.31.0026, and the HSE University Basic Research Program, Moscow; University of Tabuk research Grants No. S-1440-0321, No. S-0256-1438, and No. S-0280-1439 (Saudi Arabia); the Slovenian Research Agency Grants No. J1-9124 and No. P1-0135; Ikerbasque, Basque Foundation for Science, Spain; the Swiss National Science Foundation; the Ministry of Education and the Ministry of Science and Technology of Taiwan; and the United States Department of Energy and the National Science Foundation.

[1] E. Aprile *et al.* (XENON100 Collaboration), Phys. Rev. Lett. **109**, 181301 (2012).
[2] R. Agnese *et al.* (SuperCDMS Collaboration), Phys. Rev. Lett. **112**, 241302 (2014).
[3] D. Curtin *et al.*, Phys. Rev. D **90**, 075004 (2014).
[4] C. Bird, P. Jackson, R. Kowalewski, and M. Pospelov, Phys. Rev. Lett. **93**, 201803 (2004).
[5] C. Bird, R. Kowalewski, and M. Pospelov, Mod. Phys. Lett. A **21**, 457 (2006).
[6] M. Pospelov, A. Ritz, and M. Voloshin, Phys. Lett. B **662**, 53 (2008).
[7] N. Arkani-Hamed, D. P. Finkbeiner, T. R. Slatyer, and N. Weiner, Phys. Rev. D **79**, 015014 (2009).
[8] E. J. Chun and J.-C. Park, J. Cosmol. Astropart. Phys. 02 (2009) 026.
[9] C. Cheung, J. T. Ruderman, L.-T. Wang, and I. Yavin, Phys. Rev. D **80**, 035008 (2009).
[10] A. Katz and R. Sundrum, J. High Energy Phys. 06 (2009) 003.
[11] D. E. Morrissey, D. Poland, and K. M. Zurek, J. High Energy Phys. 07 (2009) 050.
[12] M. Goodsell, J. Jaeckel, J. Redondo, and A. Ringwald, J. High Energy Phys. 11 (2009) 027.
[13] M. Baumgart, C. Cheung, J. T. Ruderman, L.-T. Wang, and I. Yavin, J. High Energy Phys. 04 (2009) 014.
[14] Y. Nomura and J. Thaler, Phys. Rev. D **79**, 075008 (2009).
[15] D. S. Alves, S. R. Behbahani, P. Schuster, and J. G. Wacker, Phys. Lett. B **692**, 323 (2010).
[16] J. Jaeckel and A. Ringwald, Annu. Rev. Nucl. Part. Sci. **60**, 405 (2010).
[17] G. W. Bennett *et al.* (Muon $g-2$ Collaboration), Phys. Rev. D **73**, 072003 (2006).
[18] V. Barger, C.-W. Chiang, W.-Y. Keung, and D. Marfatia, Phys. Rev. Lett. **106**, 153001 (2011).
[19] T. Aoyama *et al.*, Phys. Rep. **887**, 1 (2020).
[20] B. Abi *et al.* (Muon $g-2$ Collaboration), Phys. Rev. Lett. **126**, 141801 (2021).
[21] X.-G. He, G. C. Joshi, H. Lew, and R. R. Volkas, Phys. Rev. D **43**, R22 (1991).
[22] X.-G. He, G. C. Joshi, H. Lew, and R. R. Volkas, Phys. Rev. D **44**, 2118 (1991).
[23] W. Altmannshofer, S. Gori, M. Pospelov, and I. Yavin, Phys. Rev. Lett. **113**, 091801 (2014).
[24] B. Shuve and I. Yavin, Phys. Rev. D **89**, 113004 (2014).
[25] R. Essig, P. Schuster, and N. Toro, Phys. Rev. D **80**, 015003 (2009).
[26] J. P. Lees *et al.* (*BABAR* Collaboration), Phys. Rev. Lett. **113**, 201801 (2014).
[27] B. Shuve (private communication).

[28] D. Curtin, R. Essig, S. Gori, and J. Shelton, J. High Energy Phys. 02 (2015) 157, Equation 2.12.
[29] K. Asai, K. Hamaguchi, N. Nagata, S.-Y. Tseng, and K. Tsumura, Phys. Rev. D **99**, 055029 (2019).
[30] K. Asai, K. Hamaguchi, and N. Nagata, Eur. Phys. J. C **77**, 763 (2017).
[31] E. Ma, D. P. Roy, and S. Roy, Phys. Lett. B **525**, 101 (2002).
[32] I. Adachi *et al.* (Belle II Collaboration), Phys. Rev. Lett. **124**, 141801 (2020).
[33] J. P. Lees *et al.* (*BABAR* Collaboration), Phys. Rev. D **94**, 011102 (2016).
[34] A. Abashian *et al.* (Belle Collaboration), Nucl. Instrum. Methods Phys. Res., Sect. A **479**, 117 (2002).
[35] J. Brodzicka *et al.*, Prog. Theor. Exp. Phys. **2012**, 4D001 (2012).
[36] S. Kurokawa and E. Kikutani, Nucl. Instrum. Methods Phys. Res., Sect. A **499**, 1 (2003).
[37] T. Abe *et al.*, Prog. Theor. Exp. Phys. **2013**, 3A001 (2013).
[38] A. J. Bevan *et al.*, Eur. Phys. J. C **74**, 3026 (2014), chapter 2.2.2
[39] W. Kilian, T. Ohl, and J. Reuter, Eur. Phys. J. C **71**, 1742 (2011).
[40] R. Brun, F. Bruyant, M. Maire, A. C. McPherson, and P. Zanarini, GEANT 3: User's guide Geant 3.10, Geant 3.11; rev. version, CERN, Geneva, 1987.
[41] F. Berends, P. Daverveldt, and R. Kleiss, Nucl. Phys. **B253**, 441 (1985).
[42] P. Zyla *et al.* (Particle Data Group), Prog. Theor. Exp. Phys. **2020**, 083C01 (2020).
[43] T. Skwarnicki, A study of the radiative CASCADE transitions between the Upsilon-Prime and Upsilon resonances, Ph.D. thesis Cracow, INP, 1986.
[44] G. D'Agostini, *Bayesian Reasoning in Data Analysis: A Critical Introduction* (World Scientific, Singapore, 2003).
[45] L. Moneta *et al.*, Proc. Sci. ACAT2010 (**2010**) .
[46] S. S. Gribanov and A. S. Popov, J. High Energy Phys. 11 (2021) 203.
[47] D. Geiregat *et al.*, Phys. Lett. B **245**, 271 (1990).
[48] S. R. Mishra *et al.* (CCFR Collaboration), Phys. Rev. Lett. **66**, 3117 (1991).
[49] Y. Jho, Y. Kwon, S. C. Park, and P.-Y. Tseng, J. High Energy Phys. 10 (2019) 168.
[50] Y. Kaneta and T. Shimomura, Prog. Theor. Exp. Phys. **2017**, 053B04 (2017).
[51] T. Araki, S. Hoshino, T. Ota, J. Sato, and T. Shimomura, Phys. Rev. D **95**, 055006 (2017).